Normal-incidence left-handed metamaterials based on symmetrically connected split-ring resonators

Jiafu Wang,[1] Shaobo Qu,[1,2] Zhuo Xu,[2] Hua Ma,[1,2] Song Xia,[2] Yiming Yang,[1] Xiang Wu,[1] Qian Wang,[3] and Chunhui Chen[1]
[1]*College of Science, Air Force Engineering University, Xi'an, 710051 Shaanxi, China*
[2]*Electronic Materials Research Laboratory, Key Laboratory of the Ministry of Education, Xi'an Jiaotong University, Xi'an, 710049 Shaanxi, China*
[3]*College of Environment and Planning, Liaocheng University, Liaocheng, 252000 Shandong, China*
(Received 9 December 2009; published 3 March 2010)

Normal-incidence left-handed metamaterials (LHMs) based on symmetrically connected split-ring resonators (SC-SRRs) were proposed and investigated numerically and experimentally. The SC-SRR, which can be easily fabricated by conventional printed circuit board technology, is composed of metallic patterns connected by metalized vias through the dielectric substrate. Under normal incidence, SC-SRR exhibits strong magnetic response, leading to negative permeability. By combing SC-SRRs with metallic wires, a normal-incidence LHM was realized. Both the simulation and experiment results demonstrated left-handed properties of the SC-SRR/wire LHM. The design method paved new ways of realizing magnetic and even electric metamaterials.

DOI: 10.1103/PhysRevE.81.036601 PACS number(s): 41.20.Jb, 42.25.Bs, 42.70.Qs, 73.20.Mf

I. INTRODUCTION

Left-handed metamaterials (LHMs) have many exotic properties that are beyond natural regular materials [1]. Under the long-wavelength limit, LHMs can be described by the effective medium theory [2,3]. The first LHM was composed of periodically arranged split-ring resonators (SRRs) and conducting wires [4]. Soon later, many LHMs were proposed [5–8] and most of them are variations of the SRR/wire structure. For these LHMs, the magnetic fields are required to thread through the metallic patterns to obtain a negative permeability. This brings an annoying problem: incident waves must be in parallel with substrates. This makes it quite troublesome to fabricate and use these LHMs. Dealing with this problem, Starr *et al.* proposed a normal-incidence LHM by the use of vias to form SRRs in the direction perpendicular to the substrates [9,10]. Nevertheless, there is still a saturation of the magnetic response for SRRs at optical frequencies [11]. To overcome the saturation problems, Soukoulis *et al.* proposed normal-incidence LHMs based on simple metallic pattern pairs [12–14]. Such LHMs allow normal incidence and can be conveniently fabricated and used. However, since the coupling between the metallic pattern pairs is quite weak, the left-handed properties are sensitive to the distance between neighboring unit cells along the propagation direction. Effective refractive index can be totally different for weakly and strongly coupled modes [15].

Three methods are mostly used by researchers to demonstrate a LHM. The fist one is to show and compare the transmission spectra of the LHM and its individual inclusions. By making a comparison between transmission spectra, left-handed bands can be determined qualitatively [16,17]. The second method is to retrieve the effective material parameters from simulated or measured scattering parameters [18–21]. It is now the most convenient method to characterize LHMs quantitatively and has been used to design invisible cloaks [22] and ultrathin absorbers [23]. The third method is to demonstrate negative refraction by a wedge or slab sample. If negative refraction happens, the designed structure is considered as a LHM. However, negative refraction alone is insufficient to demonstrate the left-handedness, since it can also be produced by other means such as anisotropy [24–26], chirality [27–29], and photonic crystals [30–32]. In order to sufficiently demonstrate the left-handedness, we have to observe whether the phase velocity is negative (to exclude anisotropy and chirality) and whether the wavelength is much larger than the unit cell (to exclude photonic crystals) inside the wedge or slab sample.

In this paper, we proposed normal-incidence LHMs based on SC-SRRs. The SC-SRR is composed of metallic patterns connected by metalized vias through the dielectric substrate. Under normal incidence, SC-SRR exhibits strong magnetic response. Equivalent circuit model was set up to describe the strong magnetic response. By combing SC-SRRs with metallic wires, a normal-incidence LHM was realized. Both the simulation and experiment results verified negative permeability of SC-SRR and left-handed properties of the SC-SRR/wire LHM.

II. NUMERICAL RESULTS AND ANALYSIS

A. Strong magnetic response of SC-SRRs

The most famous normal-incidence magnetic metamaterials (MMs) are based on simple metallic pattern pairs [12–14]. The magnetic response stems from the displacement current loop formed between metallic pattern pairs. When many layers of such MMs are stacking closely with a comparatively small spacing in the propagation direction, the coupling between neighboring layers reduce or even cancel that between metallic pattern pairs. Consequently, the negative magnetic response is quite sensitive to the spacing between neighboring layers [15,33].

To overcome this problem, the first idea that comes naturally is to enhance the coupling between metallic pattern pairs. There is no more straightforward way than to connect

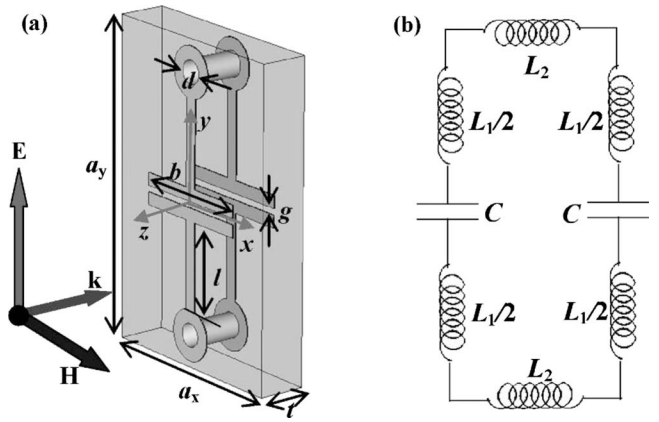

FIG. 1. The structure (a) and equivalent circuit (b) of the SC-SRR unit cell. Geometrical parameters of the SC-SRR are: $d=0.8$ mm, $b=4$ mm, $l=2.5$ mm, $g=0.2$ mm. The periodicities along x and y directions are determined by the sizes of substrates $a_x=6.7$ mm and $a_y=10$ mm, respectively. The periodicity along z directions are determined by the thickness $t=1.5$ mm of substrate as well as the spacing $s=2$ mm between neighboring layers along z directions, that is, $a_z=t+s=3.5$ mm.

the metallic pattern pair by metalized vias. This can be done easily by conventional printed circuit board (PCB) technology. Because the resulted structures are symmetrically connected by metalized vias through the substrate, we can call them symmetrically connected split-ring resonators (SC-SRRs). Figure 1(a) shows the structure of the SC-SRR. Identical copper ($\sigma=5.8\times10^7$ S/m) patterns (strip width $w=0.4$ mm, thickness $h=0.030$ mm) are etched on both sides of Teflon substrate ($\varepsilon_r=2.08$, $\tan\delta=0.0004$). The copper patterns are connected by two metalized vias. Corresponding to each part of the SC-SRR, the equivalent circuit can be described by Fig. 1(b), where C is the effective capacitance between the two parallel horizontal strips, L_1 is the effective inductances of the strip connecting the horizontal strip and metalized via, and L_2 is the effective inductances of the metalized via. When electromagnetic (EM) waves are incident onto SC-SRRs, a current loop is formed on the surface of SC-SRR, as shown in Fig. 2(a). The current loop can be considered as a magnetic dipole. Typically, the resonance behavior of a magnetic dipole can be described by the Lorentz model,

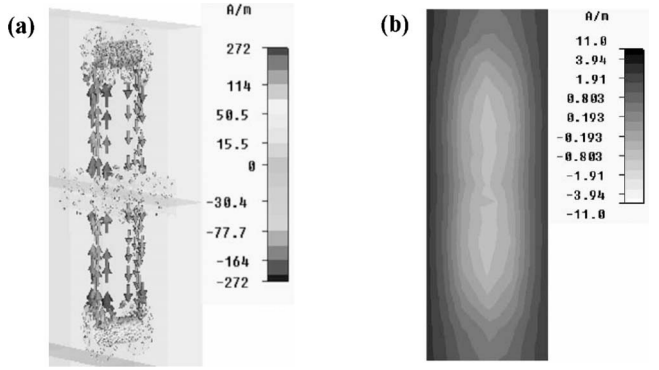

FIG. 2. Surface current on SC-SRR (a) and magnetic field distribution in (y,z) plane.

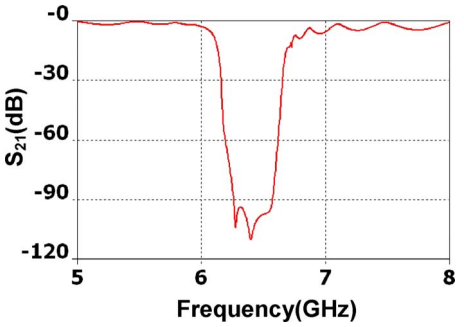

FIG. 3. (Color online) Transmission spectra for a 20-layer SC-SRR slab.

$$\mu_r = 1 - \frac{F\omega^2}{\omega^2 - \omega_m^2 + i\omega\gamma_m}, \tag{1}$$

where $\omega_m=1/\sqrt{(L_1+L_2)C}$. The current loop can produce strong magnetic field that is antiparallel with the incident magnetic field, as shown in Fig. 2(b). When the induced antiparallel magnetic field outgrows the incident magnetic field, the effective permeability μ_r becomes negative.

In the negative permeability range, EM waves cannot propagate in SC-SRRs but are reflected. Figure 3 gives the simulated transmission spectra for 20 layers of SC-SRRs stacked along the propagation direction with a spacing $s=2$ mm. The simulations were carried out using the frequency domain solver of CST Microwave Studio. The four lateral boundaries along the x and y directions are periodic boundary conditions. EM waves were incident along $-z$ direction. Thus, there are infinite unit cells in the x and y directions while 20 unit cells in the z direction. As shown in Fig. 3, there is a deep dip (below ~-60 dB) for the transmission in 6.2–6.6 GHz, which indicates strong magnetic resonance in this range.

B. Magnetic response dependent on geometrical parameters of SC-SRRs

To interpret the dependence of the magnetic resonance frequency on the geometrical parameters, the equivalent circuit model can be used to calculate the magnetic resonance frequency

$$f_m = \frac{\omega_m}{2\pi} = \frac{1}{2\pi\sqrt{(L_1+L_2)C}}.$$

The capacitance between two parallel metallic strips can be written as [34]

$$C \approx \frac{2b}{\pi}\varepsilon_0\varepsilon_r' \operatorname{arccos} h\left(\frac{2w}{g}\right), \tag{2}$$

where w, b, and g are the strip width, length, and distance of the two parallel metallic strips, respectively. ε_r' is the relative permittivity and $1<\varepsilon_r'<2.08$. The inductance of the metallic strips connecting the horizontal bars and metalized vias is approximately [35]

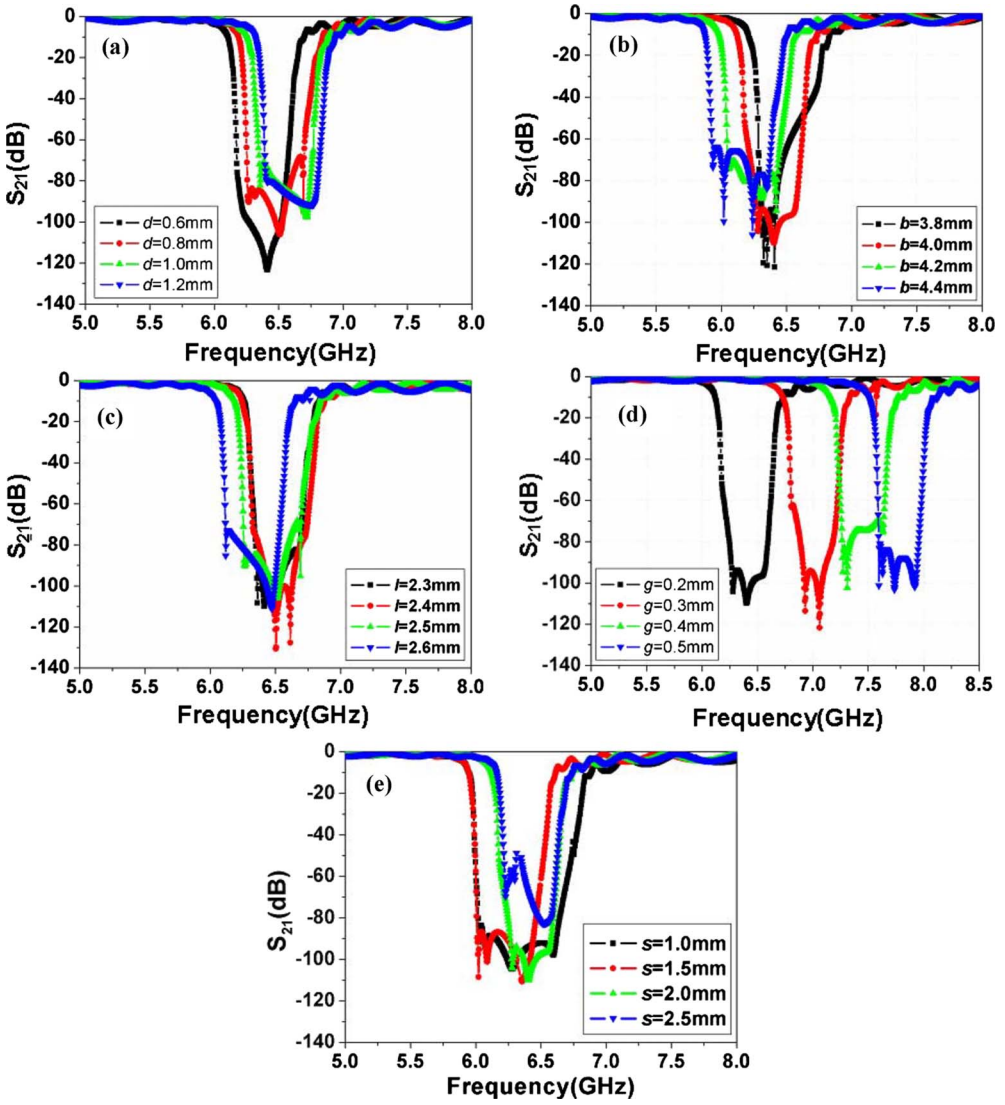

FIG. 4. (Color online) Magnetic response of SC-SRRs dependent on (a) the metalized via diameter, (b) length of horizontal bars, (c) length of the strip connecting metalized vias and horizontal bars, (d) distance between the two horizontal bars, and (e) spacing between neighboring layers.

$$L_1 \approx \frac{l\mu_0}{\pi}\ln\left(\frac{6.6l}{w+h}\right). \tag{3}$$

Because the currents between two metalized vias are antiparallel [as shown in Fig. 2(a)], the inductance of the metalized via is

$$L_2 \approx \frac{t\mu_0}{\pi}\ln\left[\frac{4(l+w)}{d}\right]. \tag{4}$$

Consequently, the magnetic resonant frequency is

$$f_m \approx \frac{c_0}{\sqrt{8b\varepsilon_r'\left(l\ln\left(\frac{6.6l}{w+h}\right)+t\ln\left[\frac{4(l+w)}{d}\right]\right)\arccos h\left(\frac{2w}{g}\right)}}, \tag{5}$$

where c_0 is the light speed in free space.

Figure 4 presents the relations between the magnetic resonance and geometrical parameters. Figure 4(a) gives the dependence of magnetic resonance on metalized via diameters. As shown in Fig. 4(a), the magnetic resonance frequency shift upwards as the via diameter increases. Because L_2 decreases with d [see Eq. (4)], the magnetic resonance frequency increases with via diameters. Note the magnetic resonance frequency is quite insensitive to via diameters. Figure 4(b) shows that the magnetic resonance frequency shift downwards as b increases. As is indicated by Eq. (2), longer bar length means larger capacitance and lower magnetic resonance frequency. Similarly, Eq. (3) indicates that when l increases, the inductance L_1 also increases. This leads to lower magnetic frequencies, as shown in Fig. 4(c). Figure 4(d) shows that the magnetic resonance frequency is very sensitive to the distance g. With a minor increment of g, the magnetic resonance frequency shift upwards significantly.

Figure 4(e) shows the dependence of the magnetic resonance of SC-SRRs on different spacings between neighboring layers along the propagation direction. As shown in Fig.

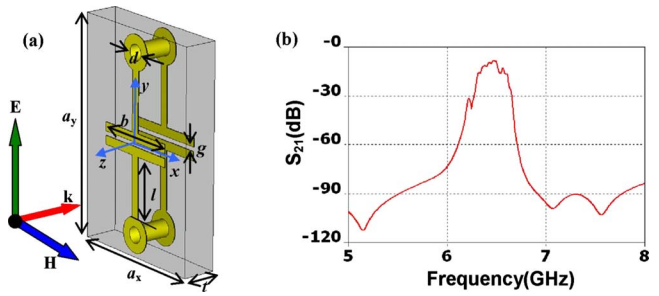

FIG. 5. (Color online) (a) The SC-SRR/wire LHM unit cell; (b) transmission spectra for 20-layer slab sample under normal incidence.

4(e), there is always a deep transmission dip in the transmission spectra for different spacings. This indicates that there is always strong negative magnetic resonance when the spacing varies between 1 mm and 2.5 mm. Note the negative bandwidth decreases with the spacing. Although the negative bandwidth changes with the spacing, the central negative resonance frequency keeps almost the same, which is consistent with Eq. (5).

C. SC-SRR/wire LHMs

Now that SC-SRRs have strong magnetic response, LHMs can be realized when they are combined with continuous wires. Figure 5(a) gives the structure of the SC-SRR/wire LHM unit cell. Copper wires of a width 0.8 mm are etched symmetrically on both sides of the substrate. When EM waves are incident, Drude-like resonance occurs in the copper wires, leading to negative permittivity. Plus negative permeability realized by SC-SRRs, double-negative property can be realized. Figure 5(b) gives the simulated transmission spectra for 20-layer LHM slab under normal incidence. As shown in Fig. 5(b), the stop band in Fig. 3 for the SC-SRR-only case is replaced by a pass band for the SC-SRR/wire LHM. This means that the pass band is left-handed.

Figure 6(a) illustrates negative phase velocity at 6.5 GHz in the 20-layer LHM slab sample by giving the time evolution of the electric field in the plane $y=4.8$ mm under normal incidence. As shown in Fig. 6(a), the phase velocity in free space advances toward $-z$ directions while that in the LHM slab toward $+z$ direction. This means that the phase velocity in the LHM slab is negative. Note the wavelength in the LHM slab spans over about ten unit cells, so the long-wavelength limit is strictly satisfied. Since the periodicity along the propagation direction is 3.5 mm, the wavelength in LHM slab is $\lambda \approx 35$ mm. The wavelength in free space at 6.5 GHz is $\lambda_0 \approx 46$ mm. Then, we can obtain the refractive index by $n=-\lambda_0/\lambda$, that is, the refractive index at 6.5 GHz of the LHM slab is about $n=-1.3$. To further demonstrate negative refraction by the LHM slab, we also simulated the LHM slab under a tilted incidence angle $\theta_i=15°$. The simulated result is shown in Fig. 6(b). According to the wave fronts indicated by localized field with the same intensity and phase, we can obtain the refracted angle $\theta_r \approx -11.5°$. According to Snell's law, the refractive index at 6.5 GHz is $n=\sin\theta_i/\sin\theta_r \approx -1.3$. The simulated results under normal and tilted incidences agree perfectly with each other.

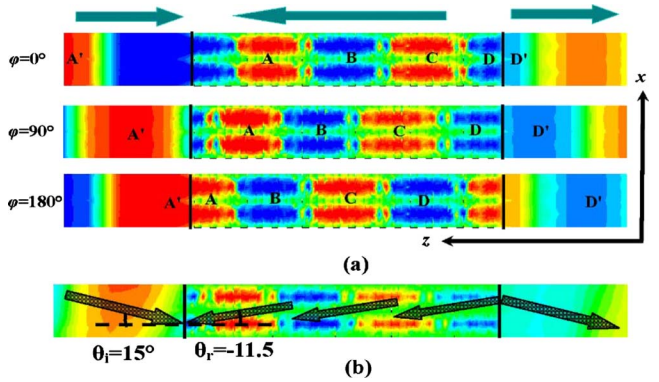

FIG. 6. (Color online) Negative phase velocity and negative refraction at 6.5 GHz in a slab sample. (a) Time evolution of the electric field distribution under normal incidence; (b) Electric field distribution under a tilted incidence angle $\theta_i=15°$. The dark solid lines indicate the free space-LHM interface and the arrows indicate the direction of phase velocity.

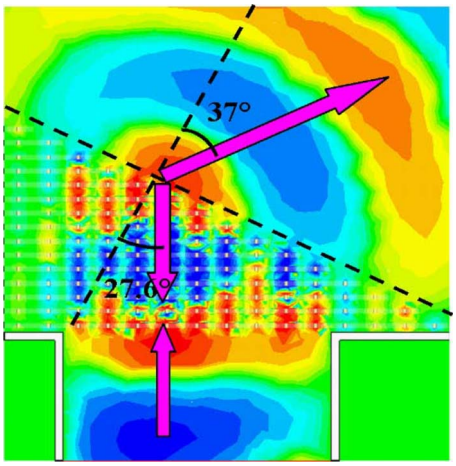

FIG. 7. (Color online) Negative phase velocity and negative refraction at 6.5 GHz in the wedge sample.

To further verify negative phase velocity and negative refraction for the SC-SRR/wire LHM, we also simulated a wedge LHM sample. The wedge sample is composed of 15 $\times$ 15 unit cells in x and z directions with one-unit-cell stairs. Figure 7 shows the simulated results for the wedge sample by giving the electric field distribution at 6.5 GHz in the plane $y=4.8$ mm. Since the periodicities along x and z directions are $a_x=6.7$ mm and $a_z=3.5$ mm, the incidence angle can be determined as $\theta_i=\arctan(a_z/a_x) \approx 27.6°$. By the localized field with the same intensity and phase, we can obtain the refracted angle $\theta_r \approx -37°$. Then, according to Snell's law, the refractive index at 6.5 GHz is $n=\sin\theta_r/\sin\theta_i \approx -1.3$. Moreover, the phase velocity inside the wedge also advances against that in free space.

III. EXPERIMENTS

SC-SRR and SC-SRR/wire LHM samples operating at X-band (8.0–12.0 GHz) were fabricated and further measured using the waveguide-based measurement system. Fig-

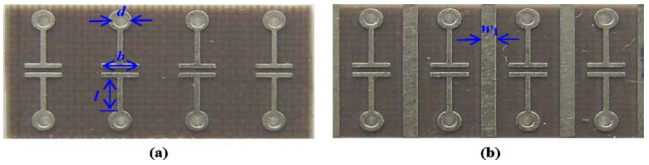

FIG. 8. (Color online) The fabricated SC-SRR and LHM layers. (a) the SC-SRR layer, (b) the LHM layer.

ures 8(a) and 8(b) shows the photos of the fabricated SC-SRR layer and the SC-SRR/wire LHM layer, respectively. Since the fabricated samples operate at X-band, the BJ-100 rectangular waveguide (8.2–12.5 GHz) with a 22.86 mm $\times$10.16 mm cross section was used in the measurement system. To fit the test sample to the waveguide cross section, four unit cells were etched on each substrate (ε_r =2.2, tan δ=0.0009) for the test samples. The substrate we used is the Rogers RT5880 (ε_r=2.2, tan δ=0.0009) substrate, whose thickness t=0.787 mm and cross section a_x $\times a_y$=20 mm$\times$10 mm. The SC-SRR is composed of copper strips (the strip width w=0.4 mm). Geometrical dimensions of the fabricated SC-SRR unit cell are: d=0.8 mm, b =2.5 mm, l=2.4 mm, g=0.3 mm. For the LHM unit cells, additional copper wires with a width w_1=1 mm were etched symmetrically with respect to SC-SRRs.

Figure 9 gives the photo, transmission spectra, and effective parameters of the SC-SRR test sample. To fabricate the SC-SRR test sample, six SC-SRR layers were stacked together with a spacing s=2 mm. One end of the six SC-SRR layers was stuck onto a thin dielectric board to fix them together, as shown in Fig. 9(a). In the measurements, the sample was put inside the waveguide to fill the cross section. HP8720ES vector network analyzer was used to measure the sample. Effective permeability and permittivity were retrieved from the measured data. Figure 9(b) gives measured scattering parameters of the SC-SRR sample. As shown in Fig. 9(b), there is a transmission dip around 10.75 GHz,

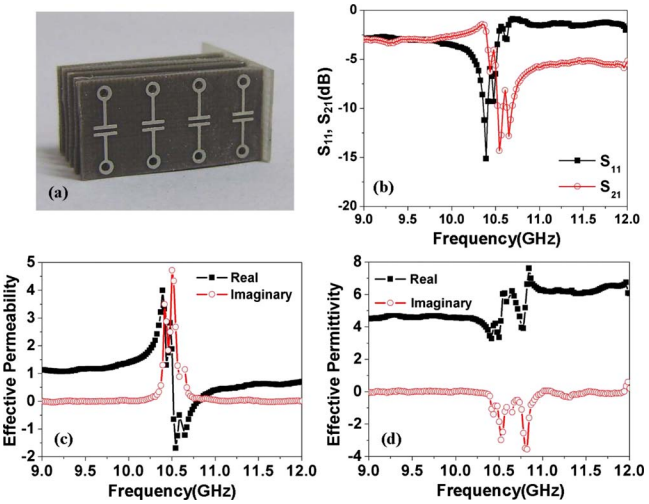

FIG. 9. (Color online) The transmission spectra and effective parameters of the SC-SRR test sample. (a) SC-SRR test sample, (b) transmission spectra, (c) effective permeability, (d) effective permittivity.

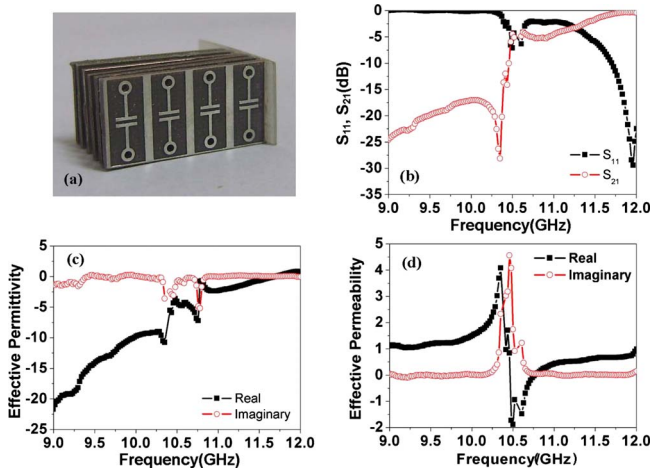

FIG. 10. (Color online) The transmission spectra and effective parameters of the LHM test sample. (a) LHM test sample, (b) transmission spectra, (c) effective permeability, (d) effective permittivity.

which indicates a single-negative region. To determine whether the effective permeability is negative, we have to resort to retrieved effective parameters. As shown in Figs. 9(c) and 9(d), the effective permeability is negative 10.5–10.8 GHz, which corresponds to the transmission dip in Fig. 9(b). Meanwhile, the effective permittivity keeps positive despite the antiresonance [20]. The measured results show that SC-SRRs can realize negative permeability under normal incidence. Compared with cut-wire pairs, the magnetic resonance of SC-SRRs is much stronger.

Figure 10 gives the photo, transmission spectra, and effective parameters of the SC-SRR/wire LHM sample. The LHM test sample is the same as the SC-SRR sample except that additional copper wires were etched symmetrically with respect to SC-SRRs, as shown in Fig. 10(a). The transmission spectra in Fig. 10(b) shows that there is a transmission peak around 10.6 GHz. Comparing Figs. 9(b) and 10(b), the transmission dip in Fig. 9(b) just corresponds to the transmission peak in Fig. 10(b). Thus, the transmission peak means a double-negative band. To determine exactly the position and bandwidth of the double-negative band, we have to resort to effective parameters retrieved from measured scattering parameters of the LHM sample. As shown in Figs. 10(c) and 10(d), the effective permittivity is negative below 11.7 GHz (the plasma frequency) while the effective permeability is negative in 10.5–10.8 GHz. Consequently, the double-negative band is 10.5–10.8 GHz and the bandwidth is 0.3 GHz. The measured results demonstrated that the SC-SRR/wire structure can realize left-handed properties under normal incidences.

IV. CONCLUSIONS

SC-SRRs can realize negative permeability under normal incidence. When combined with continuous conducting wires, SC-SRRs can be used to realize LHMs. The SC-SRR-based LHM satisfies strictly the long-wavelength limit. Simultaneously negative phase velocity and refraction were demonstrated by both the slab and wedge samples. Both the

simulation and experiment verified the strong magnetic resonance of SC-SRRs and double-negative band of the SC-SRR/wire LHM. Since SC-SRR-based LHMs allows normal incidence and can be easily fabricated by conventional PCB technology, they are of high application values in practical uses. The design method paves new ways of realizing negative permeability/permittivity metamaterials and it can be generalized to designing different kinds of magnetic metamaterials as well as electric metamateirals.

ACKNOWLEDGMENTS

This work is supported in part by the National Natural Science Foundation of China under Grants No. 50632030 and No. 60871027 and in part by the 973 Project of Science and Technology Ministry of China under Grant No. 2009CB613306. The Natural Science Foundation of Shaanxi Province, China under Grant No. SJ08F01 also supports this work.

[1] V. G. Veselago, Sov. Phys. Usp. **10**, 509 (1968).
[2] T. Koschny, M. Kafesaki, E. N. Economou, and C. M. Soukoulis, Phys. Rev. Lett. **93**, 107402 (2004).
[3] C. R. Simovski and S. A. Tretyakov, Phys. Rev. B **75**, 195111 (2007).
[4] D. R. Smith, W. J. Padilla, D. C. Vier, S. C. Nemat-Nasser, and S. Schultz, Phys. Rev. Lett. **84**, 4184 (2000).
[5] F. L. Zhang, Q. Zhao, Y. H. Liu, C. R. Luo, and X. P. Zhao, Chin. Phys. Lett. **21**, 1330 (2004).
[6] S. Xi, H. Chen, B.-I. Wu, and J. A. Kong, Prog. Electromagn. Res. **84**, 279 (2008).
[7] L. Ran, J. Huangfu, H. Chen, X. Zhang, K. Cheng, T. M. Grzegorczyk, and J. A. Kong, Prog. Electromagn. Res. **51**, 249 (2005).
[8] J. F. Wang, Sh. B. Qu, Zh. Xu, J. Q. Zhang, Y. M. Yang, H. Ma, and Ch. Gu, Photon Nanostruct. Fundam. Appl. **6**, 183 (2008).
[9] A. F. Starr, P. Rye, D. R. Smith, and S. N. Nemat-Nasser, Phys. Rev. B **70**, 113102 (2004).
[10] T. Driscoll, D. N. Basov, A. F. Starr, P. M. Rye, S. Nemat-Nasser, D. Schurig, and D. R. Smith, Appl. Phys. Lett. **88**, 081101 (2006).
[11] J. Zhou, Th. Koschny, M. Kafesaki, E. N. Economou, J. B. Pendry, and C. M. Soukoulis, Phys. Rev. Lett. **95**, 223902 (2005).
[12] J. Zhou, L. Zhang, G. Tuttle, Th. Koschny, and C. M. Soukoulis, Phys. Rev. B **73**, 041101(R) (2006).
[13] M. Kafesaki, I. Tsiapa, N. Katsarakis, Th. Koschny, C. M. Soukoulis, and E. N. Economou, Phys. Rev. B **75**, 235114 (2007).
[14] J. F. Zhou, Th. Koschny, L. Zhang, G. Tuttle, and C. M. Soukoulis, Appl. Phys. Lett. **88**, 221103 (2006).
[15] J. F. Zhou, Th. Koschny, M. Kafesaki, and C. M. Soukoulis, Phys. Rev. B **80**, 035109 (2009).
[16] R. A. Shelby, D. R. Smith, S. C. Nemat-Nasser, and S. Schultz, Appl. Phys. Lett. **78**, 489 (2001).
[17] H. S. Chen, L. X. Ran, J. T. Huangfu, X. M. Zhang, K. S. Chen, T. M. Grzegorczyk, and J. A. Kong, Appl. Phys. Lett. **86**, 151909 (2005).
[18] D. R. Smith, S. Schultz, P. Markos, and C. M. Soukoulis, Phys. Rev. B **65**, 195104 (2002).
[19] T. Koschny, P. Markos, D. R. Smith, and C. M. Soukoulis, Phys. Rev. E **68**, 065602(R) (2003).
[20] Th. Koschny, P. Markoš, E. N. Economou, D. R. Smith, D. C. Vier, and C. M. Soukoulis, Phys. Rev. B **71**, 245105 (2005).
[21] X. D. Chen, T. M. Grzegorczyk, B.-I. Wu, J. Pacheco, Jr., and J. A. Kong, Phys. Rev. E **70**, 016608 (2004).
[22] D. Schurig, J. J. Mock, B. J. Justice, S. A. Cummer, J. B. Pendry, A. F. Starr, and D. R. Smith, Science **314**, 977 (2006).
[23] N. I. Landy, C. M. Bingham, T. Tyler, N. Jokerst, D. R. Smith, and W. J. Padilla, Phys. Rev. B **79**, 125104 (2009).
[24] A. Fang, Th. Koschny, and C. M. Soukoulis, Phys. Rev. B **79**, 245127 (2009).
[25] M. G. Silveirinha, Phys. Rev. B **79**, 153109 (2009).
[26] T. G. Mackay and A. Lakhtakia, Phys. Rev. B **79**, 235121 (2009).
[27] J. F. Zhou, J. F. Dong, B. N. Wang, Th. Koschny, M. Kafesaki, and C. M. Soukoulis, Phys. Rev. B **79**, 121104(R) (2009).
[28] S. Zhang, Y.-S. Park, J. S. Li, X. C. Lu, W. L. Zhang, and X. Zhang, Phys. Rev. Lett. **102**, 023901 (2009).
[29] W. T. Dong and L. Gao, J. Appl. Phys. **104**, 023537 (2008).
[30] Y. J. Huang, W. T. Lu, and S. Sridhar, Phys. Rev. A **76**, 013824 (2007).
[31] P. V. Parimi, W. T. Lu, P. Vodo, J. Sokoloff, J. S. Derov, and S. Sridhar, Phys. Rev. Lett. **92**, 127401 (2004).
[32] E. Cubukcu, K. Aydin, E. Ozbay, S. Foteinopoulou, and C. M. Soukoulis, Nature (London) **423**, 604 (2003).
[33] J. F. Zhou, Th. Koschny, M. Kafesaki, and C. M. Soukoulis, Photon Nanostruct. Fundam. Appl. **6**, 96 (2008).
[34] B. Sauviac, C. R. Simovski, and S. A. Tretyakov, Electromagnetics **24**, 317 (2004).
[35] I. Bahl and P. Bhartia, *Microwave Solid State Circuit Design* (Wiley, New Jersey, 2003).